Supporting Information

Catalytic Mechanism of Spinel Oxides for Oxidative Electrolyte Decomposition in Mg Rechargeable Batteries

Jonghyun Han[a], Shunsuke Yagi[a], Hirokazu Takeuchi[b], Masanobu Nakayama[b,c], Tetsu Ichitsubo[d]*

[a]*Institute of Industrial Science, The University of Tokyo, 4-6-1 Komaba, Meguro-ku, Tokyo 153-8505, Japan*

[b]*Department of Advanced Ceramics, Nagoya Institute of Technology, Gokiso, Showa, Nagoya, Aichi 466-8555, Japan*

[c]*Department of Frontier Materials, Nagoya Institute of Technology, Gokiso, Showa, Nagoya, Aichi 466-8555, Japan*

[d]*Institute for Materials Research, Tohoku University, 2-1-1 Katahira, Aoba-ku, Sendai 980-8577, Japan*

*Corresponding author E-mail address: syagi@iis.u-tokyo.ac.jp

Table S1. Surface energies calculated based on density functional theory for various facets of cubic spinel-type $MgMn_2O_4$, $MgFe_2O_4$, and $MgCo_2O_4$.

Compound	Facet	Surface energy / meV Å^{-2}
$MgMn_2O_4$	100	55
	110	97
	111	738
$MgFe_2O_4$	100	75
	110	364
	111	479
$MgCo_2O_4$	100	125
	110	103
	111	615

Table S2. Lattice constants (a and c), site occupancies (g), and atomic fractional coordinates (x, y, z) of MgM_2O_4 (M = Mn, Fe, and Co) spinel oxides determined by Rietveld refinement of the synchrotron X-ray diffraction patterns shown in Figure S3.

Sample	a, c / Å	Atom	Site	g	x	y	z	B / Å^2
$MgMn_2O_4$ ($I4_1/amd$)	a = 5.72644(16) c = 9.2800(3)	Mg1	4*a*	0.864(3)	0	3/4	1/8	0.54(3)
		Mn1	4*a*	0.136	0	3/4	1/8	0.54
		Mg2	8*d*	0.068	0	0	1/2	0.451(14)
		Mn2	8*d*	0.932	0	0	1/2	0.451
		O	16*h*	1 (fixed)	0	0.4726(2)	0.25627(14)	0.58(2)
$MgFe_2O_4$ ($Fd\bar{3}m$)	8.38301(11)	Mg1	8*a*	0.024(3)	1/8	1/8	1/8	0.797(14)
		Fe1	8*a*	0.976	1/8	1/8	1/8	0.797
		Mg2	16*d*	0.488	1/2	1/2	1/2	0.338(14)
		Fe2	16*d*	0.512	1/2	1/2	1/2	0.338
		O	32*e*	1 (fixed)	0.25623(15)	0.25623	0.25623	0.46(2)
$MgCo_2O_4$ ($Fd\bar{3}m$)	8.1148(2)	Mg1	8*a*	0.4959(13)	1/8	1/8	1/8	0.277(10)
		Co1	8*a*	0.5041	1/8	1/8	1/8	0.277
		Mg2	16*d*	0.2521	1/2	1/2	1/2	0.063(7)
		Co2	16*d*	0.7479	1/2	1/2	1/2	0.063
		O	32*e*	1 (fixed)	0.26275(7)	0.26275	0.26275	0.687(16)

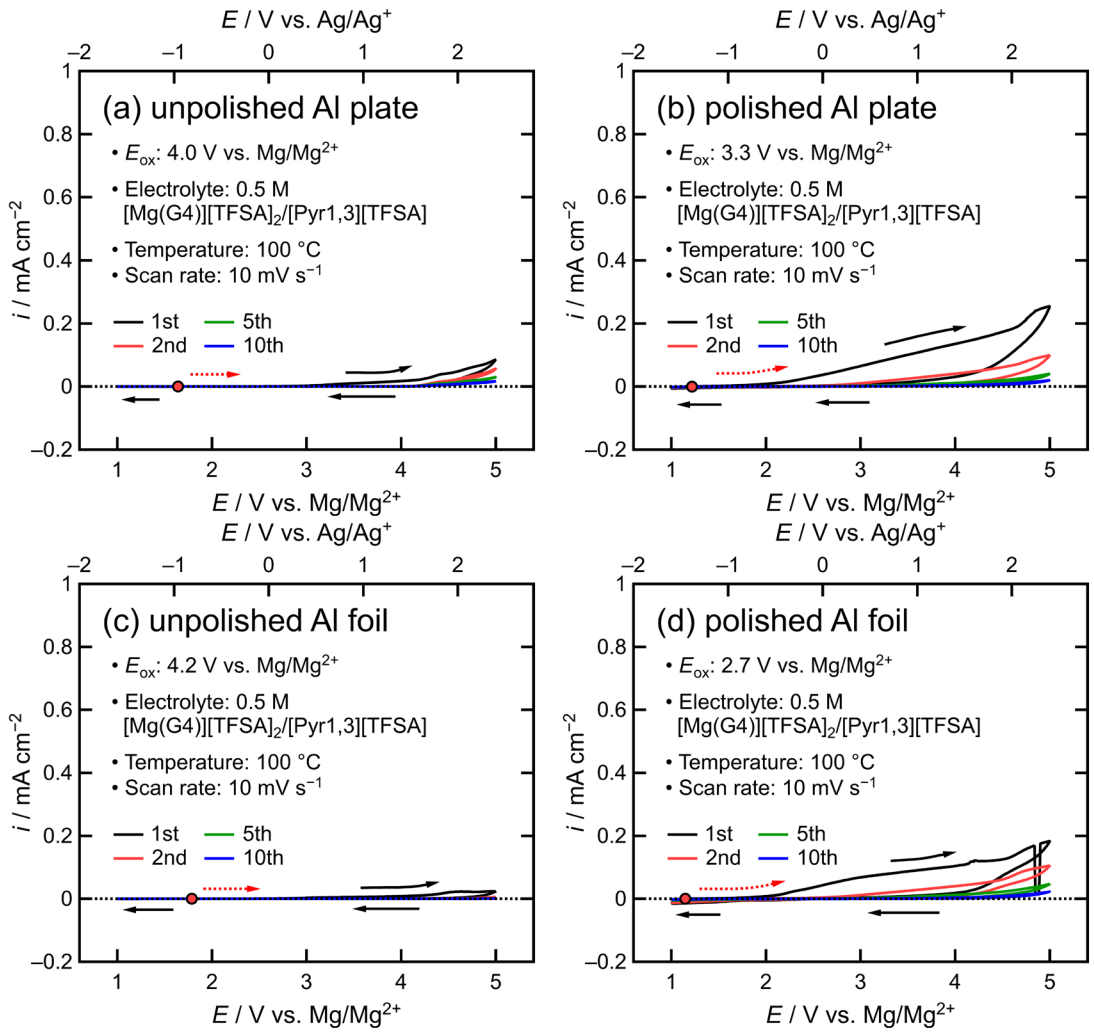

Fig. S1. Cyclic voltammograms measured using various Al electrodes as the working electrode: (a) unpolished Al plate, (b) polished Al plate, (c) unpolished Al foil, and (d) polished Al foil. Polishing was conducted using a 1200 sandpaper.

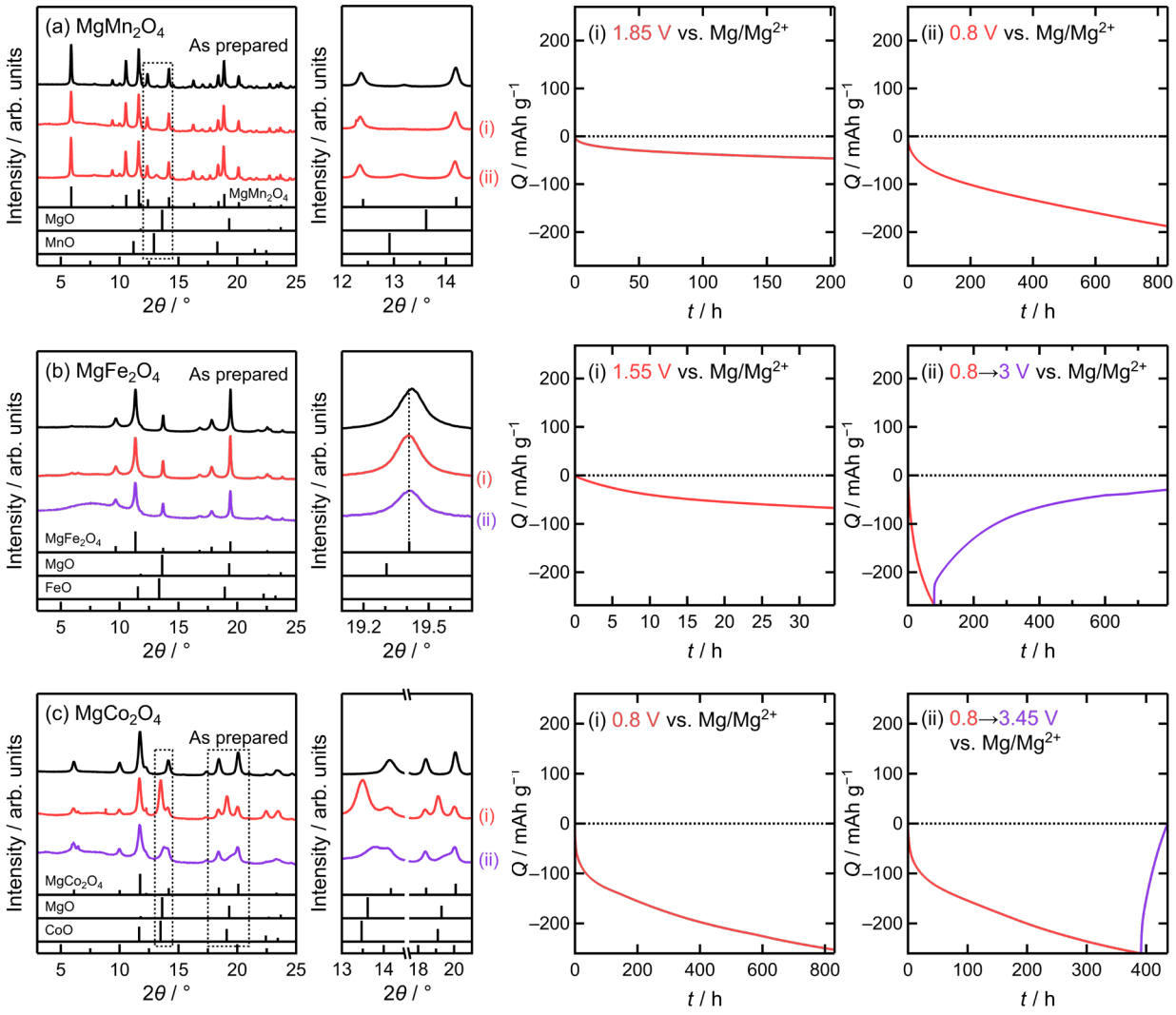

Fig. S2. Synchrotron X-ray diffraction patterns for (a) $MgMn_2O_4$, (b) $MgFe_2O_4$, and (c) $MgCo_2O_4$ before and after polarization under conditions (i) and (ii), and correspoinding chronocoulograms. The X-ray wavelength was 0.5000 Å.

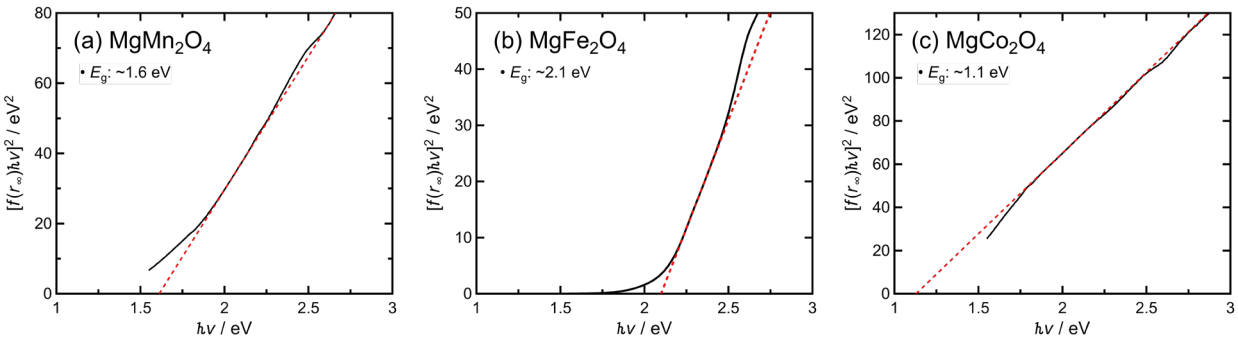

Fig. S3. Tauc plots for (a) $MgMn_2O_4$, (b) $MgFe_2O_4$, and (c) $MgCo_2O_4$, where $f(r_\infty)$ is the Kubelka-Munk function, r_∞ is the relative diffuse reflectance by UV-vis spectroscopy, and ν is the frequency of light.

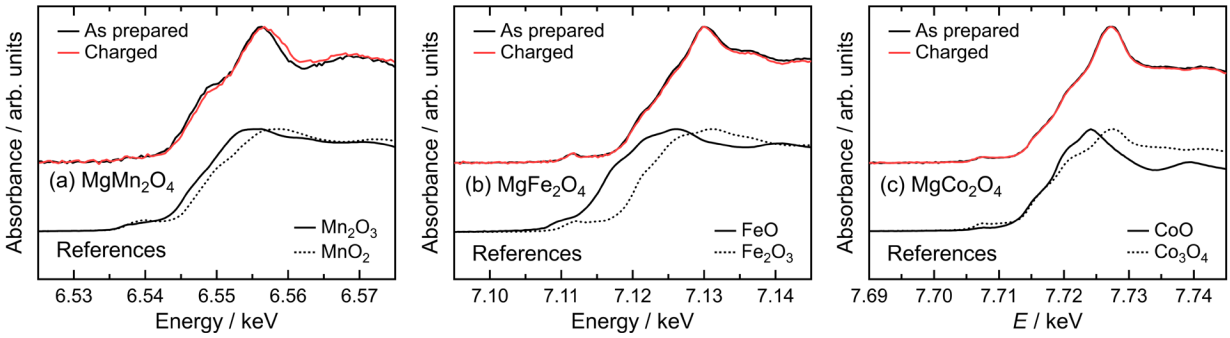

Fig. S4. X-ray absorption near-edge structure spectra for (a) $MgMn_2O_4$, (b) $MgFe_2O_4$, (c) $MgCo_2O_4$ as prepared and after the potentiostatic control at 4 V vs. Mg/Mg^{2+}. Holding time was set to be twice the time for theoretical charge completion.

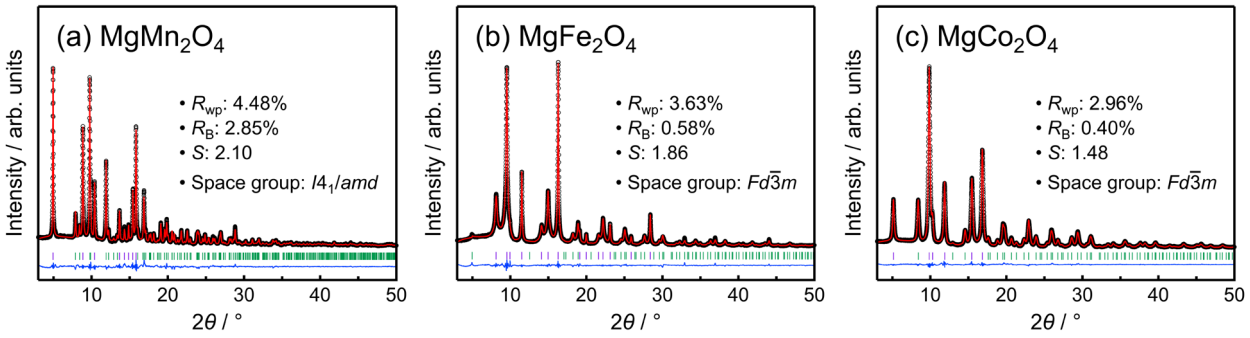

Fig. S5. Synchrotron X-ray diffraction patterns for (a) $MgMn_2O_4$ (b) $MgFe_2O_4$, and (c) $MgCo_2O_4$ spinel oxides and the corresponding fitted results by Rietveld refinement. The black open circles indicate the experimentally obtained profiles, the red lines indicate the fitted curves, and the blue lines illustrate the differences between the expeimental profiles and fitted curves. The peak positions of the expected Bragg reflections are represented using green bars, and the reflections analyzed under partial profile relaxation are represented in purple. The X-ray wavelength was 0.4200 Å.